Neuroradiology (2003) 45: 423–429
DOI 10.1007/s00234-003-0976-2

Timo Krings
Walter Möller-Hartmann
Franz-Josef Hans
Ruth Thiex
Anna Brunn
Kira Scherer
Alexander Meetz
Heiko Dreeskamp
Klaus-Peter Stein
Joachim M. Gilsbach
Armin Thron

A refined method for creating saccular aneurysms in the rabbit

Received: 30 August 2002
Accepted: 22 January 2003
Published online: 28 May 2003

T. Krings (✉) · W. Möller-Hartmann
A. Meetz · H. Dreeskamp · K.-P. Stein
A. Thron
Department of Neuroradiology,
University Hospital of the University
of Technology Aachen,
Pauwelsstrase 30, 52057 Aachen, Germany
E-mail: tkrings@izkf.rwth-aachen.de
Tel.: +49-241-8089602
Fax: +49-241-8082440

T. Krings · F.-J. Hans · R. Thiex
J.M. Gilsbach
Department of Neurosurgery, University
Hospital of the University of Technology
Aachen, Pauwelsstrase 30, 52057 Aachen,
Germany

A. Brunn
Department of Neuropathology, University
Hospital of the University of Technology
Aachen, Pauwelsstrase 30, 52057 Aachen,
Germany

K. Scherer
Department of Laboratory Animal Science,
University Hospital of the University of
Technology Aachen, Pauwelsstrase 30,
52057 Aachen, Germany

Abstract We describe a refined animal model of human intracerebral aneurysms for testing endovascular devices for interventional neuroradiological procedures. Saccular aneurysms resulting from a stump of the right common carotid artery (CCA) were created in 15 New Zealand White rabbits by intraluminal incubation of elastase that was applied to the CCA after distal ligation of the CCA and proximal occlusion of the vessel using a pliable balloon. Subsequently a microcatheter was advanced to a position cranial to the balloon and the elastase was infused under fluoroscopic guidance to avoid retrograde flow to the trachea via aberrant vessels. Contrast-enhanced (CE) MRA at 1.5 T and conventional digital subtraction angiography was performed to test for aneurysm size, morphology and neck anatomy. In all 15 animals aneurysms resulted from the stump of the right CCA, ranging in size from 2.0 to 9.9 mm (mean 6.3 mm) in craniocaudal direction, 1.0 to 5.5 mm (mean 3.8 mm) in mediolateral direction and 1.0 to 3.8 mm (mean 2.4 mm) in neck diameter. Aneurysm morphology could be adequately demonstrated using CE MRA. On histological evaluation a loss of the internal elastic lamina was noted. The described method represents an easy, reliable, and reproducible method of aneurysm creation in the rabbit in an area of high shear stress. These aneurysms can be used for testing new endovascular devices for embolization of intracranial aneurysms.

Keywords Aneurysm model
Rabbit · Elastase · Experimental
neuroradiology · Intervention

Introduction

Endovascular treatment of cerebral aneurysms has gained importance in recent years, not only for complicated aneurysms in areas difficult to access surgically, but also as an alternative treatment of uncomplicated aneurysms, since interventional neuroradiological procedures offer less invasive treatment options that also exclude an aneurysm from the cerebral circulation. The most widely used method to treat aneurysms via an endovascular approach is the Guglielmi detachable coil system (GDC) (Boston Scientific, Target, Natick, Mass.), which has gained worldwide acceptance [1, 2, 3]. However, disappointing clinical results with aneurysm recurrence due to coil compaction were observed in some studies, especially after embolization of wide-necked aneurysms [4]. To increase intra-aneurysmal fibrosis or even re-endothelialization of the parent vessel wall, coil modifications with

collagen coatings or ion implantation, new embolization devices (Onyx) and methods (coil via stent) have been developed. With the advent of these new embolization devices preclinical testing of biocompatibility has become increasingly important. Therefore, in vivo animal models of cerebral aneurysms have emerged in recent years [5, 6, 7, 8, 9, 10, 11, 12, 13, 14, 15]. Ideally, these models simulate the morphology and hemodynamics of human aneurysms. Experimentally created aneurysms should: (a) demonstrate long-term patency in untreated animals, (b) simulate aneurysm morphologies that put a high shear stress on the neck of the aneurysm (terminal or bifurcation aneurysms), (c) be of similar size (as regards both the aneurysm and the parent vessel), (d) maintain the integrity of the endothelium to minimize the release of platelet-derived growth factors that ultimately lead to scarring and obliteration of the aneurysmal cavity, (e) consist of a thin arterial wall, (f) have a rapid construction time, (g) be reliable and reproducible, and, finally, (h) be created in animals that have a coagulation system similar to that of humans [16].

At present, most aneurysm models are produced microsurgically, using venous pouches within an artificial arterial bifurcation [17]. However, these venous patch grafts require suture lines that encircle the neck of the aneurysm, which lead to a healing response obscuring the biological activity of the embolization devices [16, 18]. Recently, an aneurysm model was proposed that uses an endovascular approach to produce bifurcation aneurysms in the rabbit [12]. In this model the right common carotid artery is surgically exposed, distally ligated and a sheath is advanced retrogradely into this vessel that is subsequently occluded proximally using a pliable balloon. One hundred units of elastase are injected via the sheath and incubated within the lumen of the occluded artery for 20 min. After removal of the sheath, aneurysms begin to form within 2 weeks. One major problem of this method is the injection of elastase via the sheath, since the tendency is to push the blood column that is still present within the ligated artery but not the elastase into the lumen. Other problems include the amount of elastase which, in our experience, is often fatal to the animals, and the occurrence of anastomoses that might lead to a washout of elastase to the trachea that might also be harmful to the animals. The aim of this paper is to present a refined method of endovascular creation of aneurysms in the rabbit that takes the various problems of the previously reported model into account.

Materials and methods

The study was conducted according to current German regulations and guidelines for animal welfare (AZ: 50.203.2-AC 24, 24/01). Fifteen female New Zealand White rabbits (3.5–4.2 kg) purchased from ESD, France, were used in this study. Anesthesia was induced by intramuscular injection of 0.2 ml/kg KG ketamine (10%) and 0.3 ml/kg KG medetomidine; maintenance of anesthesia was achieved by 2.5% isoflurane inhalation. Using a sterile technique, the right carotid sheath was surgically exposed, the right common carotid artery (CCA) was isolated, and ligated

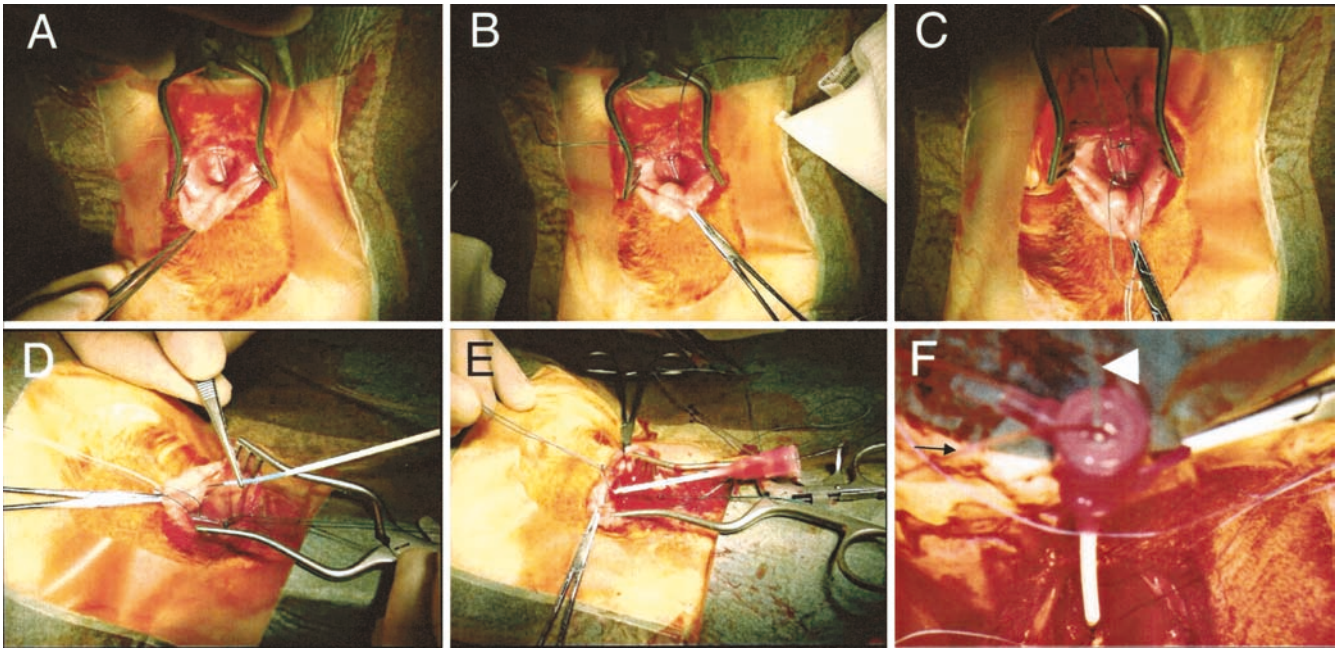

Fig. 1 Production of aneurysms in the rabbit. After surgical exposure and isolation of the right common carotid artery (**A**), distal (**B**) and proximal control of the vessel is obtained by silk sutures (**C**). An arteriotomy is performed and a 4 Fr vascular sheath is introduced retrogradely into the vessel (**D**, **E**). The sheath is tightly fixated at the vessel (**E**). Afterwards, both the balloon (*arrow* in **F**) and, subsequently, the microcatheter (*arrowhead* in **F**) are advanced via the same sheath

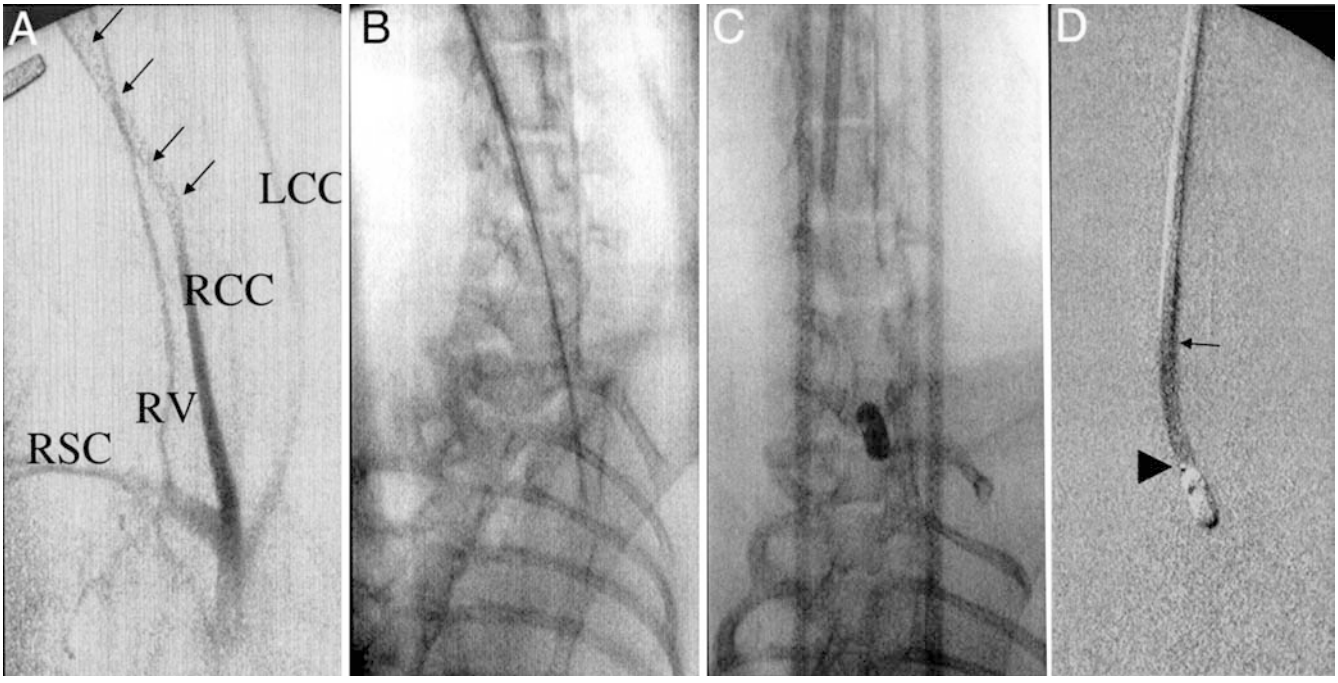

Fig. 2 Production of aneurysms in the rabbit. Before both the microcatheter and the balloon are inserted via the sheath, the vascular anatomy can be visualized by contrast injection via the sheath (*arrows* in **A**). This demonstrates the origin of the right common carotid artery (*RCC*) where the balloon should be placed subsequently. *RV*: right vertebral artery, *RSC* right subclavian artery, *LCC* left common carotid artery. Under fluoroscopic guidance, a Fogarty balloon is advanced retrograde to the origin of the RCCA from the brachiocephalic artery (**B**). Once in position, the balloon is slowly inflated with iodinated contrast material under fluoroscopic guidance (**C**). Subsequently, the microcatheter is advanced and placed directly distal to the balloon. The *arrowhead* in **D** demonstrates the tip of the microcatheter, the *arrow* the distal end of the sheath. The elastase/contrast material mixture is then injected under fluoroscopic guidance and the column can be visualized as slowly ascending to the distal end of the sheath (**D**)

distally using a 3-0 silk suture. Proximal control of the vessel was obtained with a 3-0 silk suture as well before a 1–2 mm beveled arteriotomy was made and a 4 Fr vascular sheath (Radiofocus Introducer II, Terumo, Tokyo, Japan) was passed retrograde to the mid-portion of the CCA (Fig. 1). Next, under fluoroscopic guidance, a 2 Fr Fogarty balloon (Pan Medical, Gloucestershire, UK) was advanced retrograde to the origin of the CCA from the brachiocephalic artery. Once in position, the balloon was slowly inflated with iodinated contrast material under fluoroscopic guidance (Fig. 2). Occlusion of the vessel was tested by retrograde injection of non-ionic contrast via the sheath. This test injection was also carried out to test carefully for aberrant arteries that might arise from the proximal CCA and that target the trachea. Therefore, after injection of contrast material via the sheath under digital subtraction conditions, the behavior of the contrast material was noted. Only if the column of contrast material was present for 2 min without washout or dilution, did we proceed further. In those cases where washout via aberrant vessels was noted (Fig. 3A), the sheath was further advanced retrograde to the origin of the CCA and the procedure was repeated until a satisfactory result was obtained. The column of contrast material was removed from the CCA stump via the sheath as far as possible by applying continuous suction to the sheath. In contrast to the previously described method [12], we then advanced a Tracker 10 (Boston Scientific Target, Fremont, Calif.) microcatheter supported by a Seeker light 10 (Boston Scientific Target, Fremont, Calif.) microguidewire through the same sheath, and under fluoroscopic guidance placed the microcatheter directly above (distal to) the Fogarty balloon.

Porcine elastase was mixed with equivalent amounts of non-ionic contrast-material to obtain a 50% dilution. A total of 20 units of elastase was administered. In the above-mentioned position, the elastase was injected under fluoroscopic guidance. Special points of interest were: movement of the Fogarty balloon, flow of the elastase/contrast mixture into the brachiocephalic artery, reflux through the sheath, dilatation of the CCA. Elastase was incubated for 20 min in the lumen of the artery, which was separated from the circulation by the ligation at the distal end and the Fogarty balloon at the proximal end. Thereafter, using an empty luer lock syringe, the volume remaining in the CCA was removed. Subsequently, the microcatheter was removed. Under continuous suction of the sheath, the balloon was deflated and removed. Finally, under distal control of the CCA via a 3-0 silk suture, the sheath was removed and the vessel was ligated in the mid-portion. The skin was closed with a running suture.

Aneurysms formed within the stump of the right CCA and were investigated using MR angiography (MRA) [19]. The animals were anesthetized as described above. MRA was performed using a 1.5 T Philips Gyroscan Intera (Philips Medical Systems, Best, The Netherlands; amplitude: 30 mT/m, slew rate: 150 mT/m/ms) within a commercially available knee/extremity bird-cage coil. First, phase contrast scout images in the sagittal plane were obtained. Subsequently, three-dimensional (3D) contrast-enhanced (CE) MRA was performed in the coronal plane. The sequence was started immediately after intravenous contrast medium (4 ml gadolinium DTPA) injection in an ear vein subsided. Scanning parameters were as follows: 3D T1 FFE CE angiography with linear profile order, TR/TE/FA: 4 ms/1.2 ms/30°, FOV: 260×104 mm, 40 slices, 1 mm slice thickness, 256×256 matrix. All MR angiograms were reconstructed with maximum intensity projections targeted on the vessels of interest with lateral rotation obtained by 8° increments.

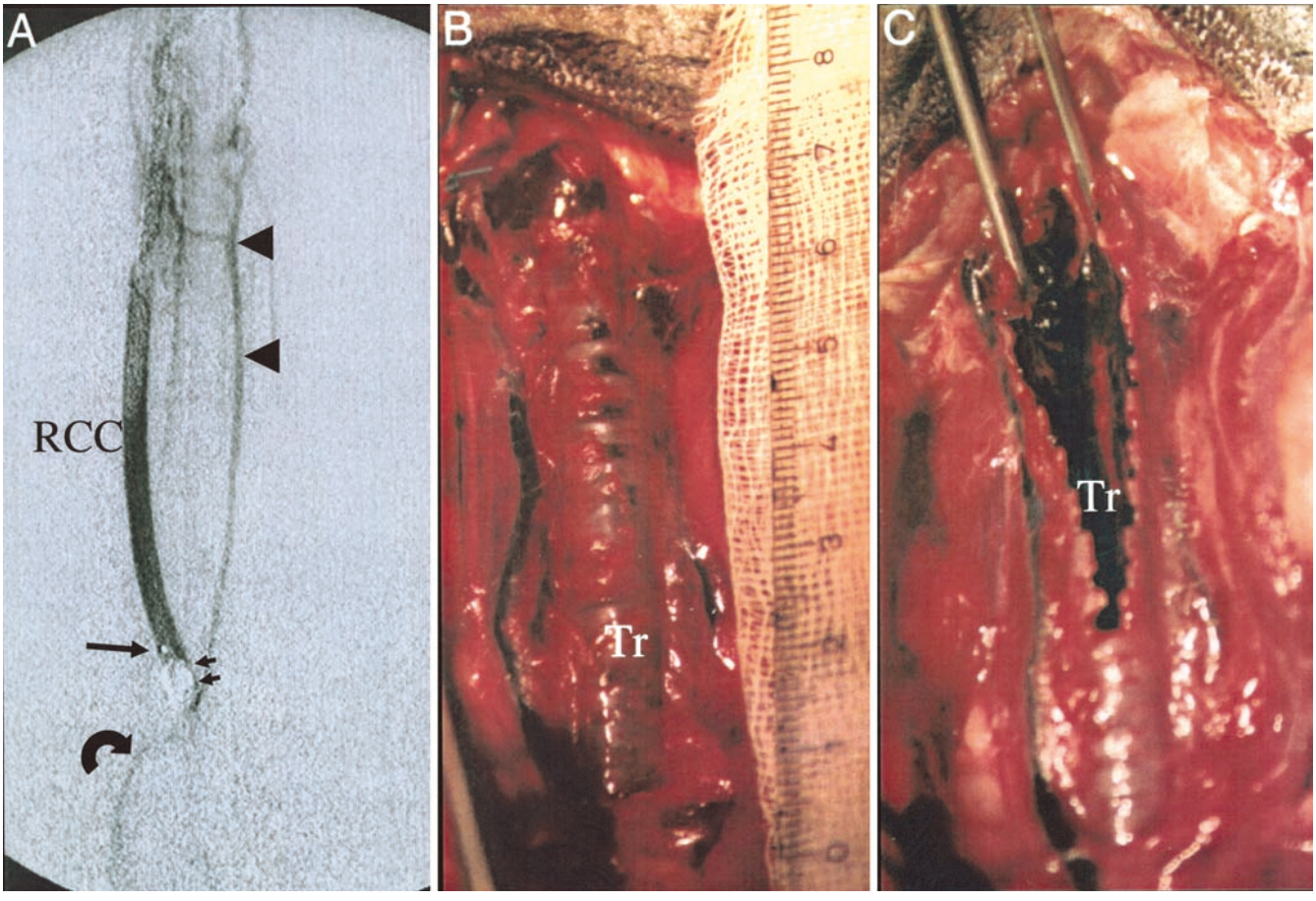

Fig. 3 Pitfalls in aneurysm creation. In this case, the test injection via the microcatheter (*large arrow* in **A**) revealed slow washout of contrast material via aberrant vessels targeting the trachea that are drained via the tracheal plexus (*arrowheads* in **A**) into the superior caval vein (*curved arrow* in **A**). The *small arrows* denote the position of the balloon. If elastase was injected in one of these cases, a hemorrhagic necrosis (**B**, **C**) of the trachea occurs within the next 24 h, due to which we lost several animals during the first experiments (**B**, **C**: autopsy photographs of the trachea, *Tr*)

Results

All animals treated with the above-described method tolerated the procedure well; no periprocedural mortality occurred. The total time to construct an aneurysm was approximately 40 min. In approximately half the animals, when performing digital subtraction angiography (DSA) through the sheath with the balloon inflated, contrast material washout via aberrant vessels to the trachea was noted. In these animals, the sheath was placed more proximally. Under fluoroscopic control, the elastase/contrast mixture was injected so that the column of contrast slowly ascended and dilated the separated CCA.

In all animals saccular or berry-shaped aneurysms were seen, both on 3D CE MRA and on conventional DSA. On 3D CE MRA, aneurysm sizes ranged in width from 1.1 mm to 5.4 mm (mean 3.6 mm, standard deviation 1.5 mm) and in height from 2.4 mm to 10.3 mm (mean 6.4 mm, standard deviation 3.7 mm). The aneurysm neck was in all cases well defined and had a diameter ranging from 1.0 mm to 4.2 mm (mean 2.6 mm, standard deviation 1.4 mm). The size of the parent artery (the brachiocephalic trunk) ranged from 2.2 mm to 4.8 mm (mean 3.4 mm, standard deviation 0.9 mm) (Figs. 4A, 5A).

DSA demonstrated similar results, with aneurysm sizes that ranged in width from 1.0 mm to 5.5 mm (mean 3.8 mm, standard deviation 1.6 mm) and in height from 2.0 mm to 9.9 mm (mean 6.3 mm, standard deviation 3.4 mm). The aneurysm neck was again in all cases well defined and had a diameter ranging from 1.0 mm to 3.8 mm (mean 2.4 mm, standard deviation 1.5 mm). The size of the parent artery (the brachiocephalic trunk) ranged from 2.8 mm to 3.6 mm (mean 3.2 mm, standard deviation 0.5 mm) (Figs. 4B, 5B).

Three animals were killed 6 months following aneurysm creation. On gross pathological inspection, the distal portion of the CCA, from the ligated portion of

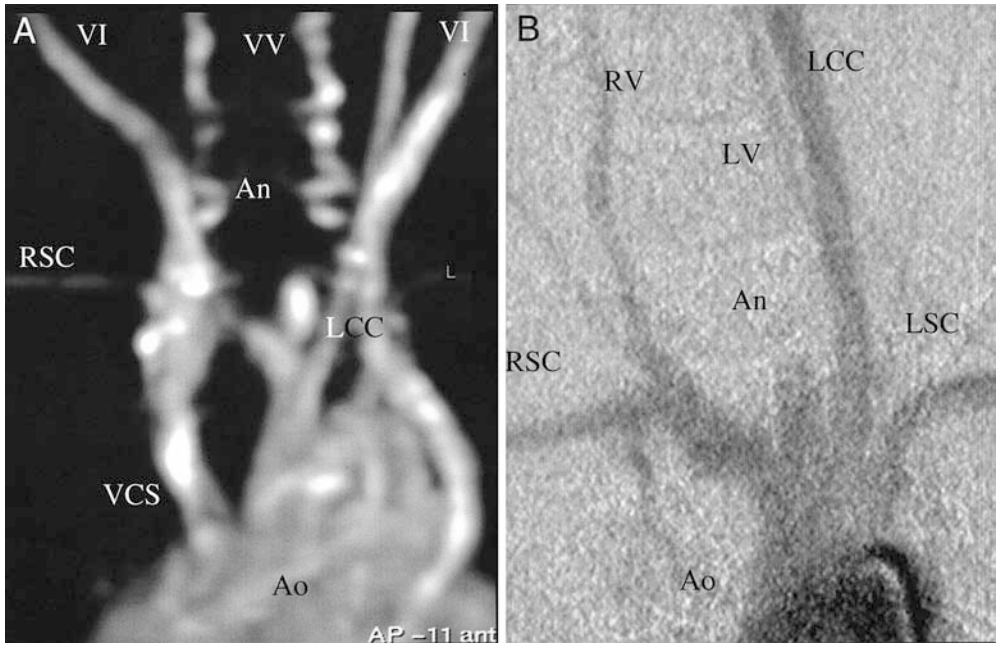

Fig. 4 MRA (**A**) and DSA (**B**) of experimentally induced aneurysms. Contrast-enhanced MRA and conventional DSA revealed a berry-shaped aneurysm that formed from the stump of the former right common carotid artery with a defined neck and a saccular configuration. *VI* jugular vein, *VV* vertebral veins, *An* aneurysm, *VCS* superior caval vein, *Ao* aorta, *LCC* left common carotid artery, *RSC*: right subclavian artery, *RV* right vertebral artery

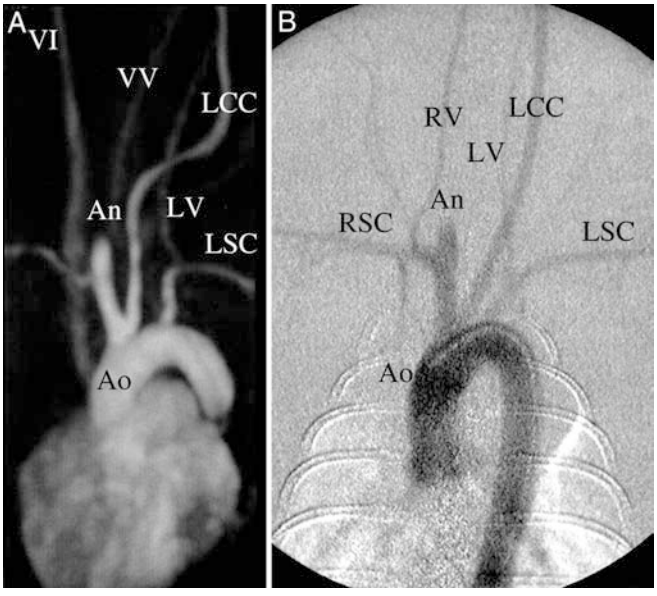

Fig. 5 MRA (**A**) and DSA (**B**) of experimentally induced aneurysms. Contrast-enhanced MRA and conventional DSA revealed a berry-shaped aneurysm in this animal as well. For abbreviations see the legend to Fig. 4

the vessel downward, was completely obliterated whereas the portion of the former vessel close to the aneurysm dome showed thrombosis (Fig. 6A). Histologically, a loss of the internal elastic lamina and a thrombosed dome was demonstrated (Fig. 6B–D).

Discussion

Before we used the above-described modified animal model, a high percentage of animals died within 24 h following the procedure. On autopsy the trachea of these animals demonstrated hemorrhagic necrosis (Fig. 3B, C). When re-evaluating aneurysm creation it was, however, noted, that a slow washout of contrast as demonstrated in Fig. 3 was present. We therefore presume that the elastase reached the trachea via these inconstant collaterals, damaged the mucosal tissue and thereby led to tracheal edema that finally killed the animals. Once this problem was identified and the aneurysm model was changed to the above-described method, no animal died but all animals still developed berry-shaped aneurysms similar in size, shape and configuration of the parent vessel to human bifurcation aneurysms.

The described method has various advantages over previously published reports on experimental aneurysm creation. (1) Most surgical models rely on venous patch grafts that are sewn on straight segments. This procedure yields a sidewall aneurysm [20]. In comparison with human intracerebral aneurysms neither the anatomical nor the hemodynamic characteristics are present. In particular shear stress forces that are normally present at the aneurysm neck in bifurcation aneurysms and that might lead to a compaction of coils over time are not present in sidewall aneurysms [16]. (2) In comparison with surgically created aneurysms, the time required to create an aneurysm is considerably shorter in our model and the technique is easier to perform. In some of these

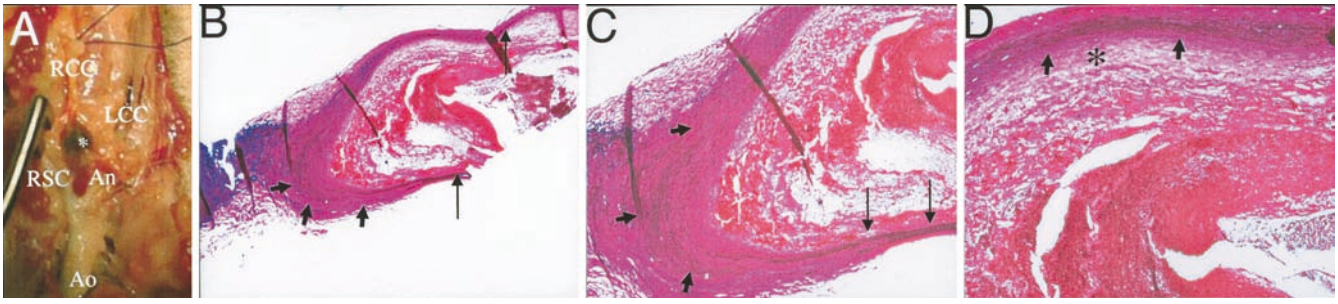

Fig. 6 Histopathological configuration of the aneurysm. The autopsy situs (**A**) demonstrates the patent left common carotid artery (*LCC*), the obliterated right common carotid artery (*RCC*), thrombus material within the aneurysm dome (*asterisk* in **A**) and the perfused aneurysm (*An*). *RSC* right subclavian artery, *Ao* aorta. The Elastica-van Gieson stain with different magnifications (**B**: ×12, **C**: ×30, **D**: ×60) demonstrates a diffuse internal elastic lamina (*small arrows*), thrombus material adherent to the aneurysm dome (*asterisk* in **D**) and a normal configuration of the arterial wall proximal to the aneurysm (*large arrows*). This demonstrates the effect of the elastase on the internal elastic lamina of the arterial wall. Thrombus material in the aneurysm dome is often encountered in human aneurysms and is not a major drawback of this model

studies high rates of mortality and inadvertent parent artery occlusion were seen [21, 22]. Furthermore, the vessel wall is venous rather than arterial, which might lead to hypertrophic changes within the venous wall. An arterial wall better simulates the morphological and histological attributes of human aneurysms [9]. Moreover, in all surgical models sutures are needed at the aneurysm neck and in most models also at the aneurysm dome. It has been found that there is extensive fibrosis and the formation of new vessels as the morphological basis of an extensive healing process around these sutures [18]. These models therefore cannot be used when testing new embolization materials that aim at improvement of intra-aneurysmal fibrosis [11]. (3) In comparison with the previously described endovascular method the proposed technique has the following advantages: in our model the elastase has the highest concentrations at the base of the CCA, that is, the area where the neck of the aneurysm forms. In the model described previously the elastase is injected via the sheath, thereby pushing a column of blood forward to the most proximal parts of the CCA. Therefore, there is a dead space without elastase at the part of the vessel that will form the neck of the aneurysm. In our model the vessel is filled retrogradely with elastase, thereby pushing the column of blood towards the sheath where the aneurysm dome will form. By mixing contrast material and elastase, it is additionally possible to visualize how the vessel is stretched. The additional DSA control performed to rule out anastomoses via aberrant vessels that run from the CCA to the trachea is in our experience absolutely necessary to check the correct position of the sheath in relation to these vessels. When these aberrant collaterals remain patent, washout of the contrast column can be appreciated; if elastase were injected in this situation, death of the animal due to elastase ingestion via the trachea might result. Moreover, in our experience 20 units of elastase instead of the 100 units formerly used are sufficient for successful and reliable aneurysm creation. On the contrary, higher doses might lead to an ingestion of tissues surrounding the CCA, which might explain why some of our animals treated in earlier stages of our experiment were in apparent distress following the endovascular procedure.

We have seen a very good correlation between CE MRA and DSA as the gold standard, with regard to both the size and neck visualization, whereas in a previous study the size was both overestimated and (more often) underestimated with time of flight (TOF) and phase contrast (PC) MRA sequences [19]. The overestimation of the aneurysm size in TOF angiography is probably due to sub-acute thrombus, which is a common cause of misinterpreted high signal. Since one property of our model is thrombus in the aneurysm dome, this might cause problems in the determination of the aneurysm size. PC and CE MRA sequences are very useful in distinguishing thrombus from flow, since PC MRA is not sensitive to the T1 shortening effect of methemoglobin while CE MRA, on the other hand, mainly depends on the concentration of contrast medium within the part of the aneurysm that is still perfused. CE MRA can be used for pre-interventional determination of aneurysm size, morphology and direction. This is especially helpful when considering the growth of aneurysms over time [23]. Moreover, the dome and the neck of the aneurysm can be identified reliably. Thereby, it is possible to determine what kind of coils are best suited for a specific aneurysm, and the treatment can be better planned pre-interventionally.

The described method is an easy and fast technique for creating aneurysms that resemble human aneurysms in size, size of the parent artery and blood flow conditions. On histological evaluation, a loss of the internal elastic lamina and a thrombosed dome was demonstrated, therefore representing a suitable model for human aneurysms, since it has been found that the morphology, cellular content and appearance of the elastic lamina in elastase-induced aneurysms are similar

to those of human cerebral aneurysms [9]. Furthermore, since thrombus is present in the aneurysm dome, our model closely resembles ruptured human aneurysms that also typically demonstrate thrombus within their dome, presenting a possible reason for later coil compaction. Our aneurysm model can, therefore, be used to test new embolization material in vivo. Collagen-coated coils can be tested as well as other coating methods that induce fibrosis or even a re-endothelialization of the aneurysm. Moreover, other methods that might lead to a reconstruction of the vessel with complete occlusion of the aneurysm, such as covered stents or coil placement via uncovered stents, can be tested and compared with conventional embolization procedures using the GDC system.

Acknowledgements We greatly appreciate the help of Dr. S. Kinzel concerning animal anesthesia and of Prof. Dr. W. Küpper, Dr. H. Kommans, Dr. C. Herweg, T. Stopinski, and I. Hermanns concerning animal care. Without their dedication this work would not have been possible. This work was supported by the Deutsche Forschungsgemeinschaft (KR 2008 4/1) and the Else Kröner-Fresenius-Stiftung.

References

1. Guglielmi G, Vinuela F, Sepetka I, Macellari V (1991) Electrothrombosis of saccular aneurysms via endovascular approach. 1. Electrochemical basis, technique, and experimental results. J Neurosurg 75: 1–7
2. Guglielmi G, Vinuela F, Dion J, Duckwiler G (1991) Electrothrombosis of saccular aneurysms via endovascular approach. 2. Preliminary clinical experience. J Neurosurg 75: 8–14
3. Guglielmi G, Vinuela F, Duckwiler G, et al (1992) Endovascular treatment of posterior circulation aneurysms by electrothrombosis using electrically detachable coils. J Neurosurg 77: 515–524
4. Malisch TW, Guglielmi G, Vinuela F, et al (1997) Intracranial aneurysms treated with the Guglielmi detachable coil: midterm clinical results in a consecutive series of 100 patients. J Neurosurg 87: 176–183
5. Massoud TF, Ji C, Guglielmi G, Vinuela F, Robert J (1994) Experimental models of bifurcation and terminal aneurysms: construction techniques in swine. AJNR Am J Neuroradiol 15: 938–944
6. Massoud TF, Guglielmi G, Ji C, Vinuela F, Duckwiler GR (1994) Experimental saccular aneurysms. I. Review of surgically-constructed models and their laboratory applications. Neuroradiology 36: 537–546
7. Powell J (1991) Models of arterial aneurysm: for the investigation of pathogenesis and pharmacotherapy—a review. Atherosclerosis 87: 93–102
8. Stehbens WE (1997) Histological changes in chronic experimental aneurysms surgically fashioned in sheep. Pathology 29: 374–379
9. Abruzzo T, Shengelaia GG, Dawson RC, 3rd, Owens DS, Cawley CM, Gravanis MB (1998) Histologic and morphologic comparison of experimental aneurysms with human intracranial aneurysms. AJNR Am J Neuroradiol 19: 1309–1314
10. Cawley CM, Dawson RC, Shengelaia G, Bonner G, Barrow DL, Colohan AR (1996) Arterial saccular aneurysm model in the rabbit. AJNR Am J Neuroradiol 17: 1761–1766
11. Cloft HJ, Altes TA, Marx WF, et al (1999) Endovascular creation of an in vivo bifurcation aneurysm model in rabbits. Radiology 213: 223–228
12. Altes TA, Cloft HJ, Short JG, et al (2000) 1999 ARRS Executive Council Award. Creation of saccular aneurysms in the rabbit: a model suitable for testing endovascular devices. American Roentgen Ray Society. AJR Am J Roentgenol 174: 349–354
13. Kallmes DF, Altes TA, Vincent DA, Cloft HJ, Do HM, Jensen ME (1999) Experimental side-wall aneurysms: a natural history study. Neuroradiology 41: 338–341
14. Miskolczi L, Guterman LR, Flaherty JD, Szikora I, Hopkins LN (1997) Rapid saccular aneurysm induction by elastase application in vitro. Neurosurgery 41: 220–228; discussion 228–229
15. Spetzger U, Reul J, Weis J, Bertalanffy H, Thron A, Gilsbach JM (1996) Microsurgically produced bifurcation aneurysms in a rabbit model for endovascular coil embolization. J Neurosurg 85: 488–495
16. Kallmes DF, Helm GA, Hudson SB, et al (1999) Histologic evaluation of platinum coil embolization in an aneurysm model in rabbits. Radiology 213: 217–222
17. Reul J, Spetzger U, Weis J, Sure U, Gilsbach JM, Thron A (1997) Endovascular occlusion of experimental aneurysms with detachable coils: influence of packing density and perioperative anticoagulation. Neurosurgery 41: 1160–1165; discussion 1165–1168
18. Mawad ME, Mawad JK, Cartwright J, Jr, Gokaslan Z (1995) Long-term histopathologic changes in canine aneurysms embolized with Guglielmi detachable coils. AJNR Am J Neuroradiol 16: 7-13
19. Krings T, Hans FJ, Moeller-Hartmann W, et al (2002) Time-of-flight, phase contrast and contrast enhanced magnetic resonance angiography for pre-interventional determination of aneurysm size, configuration, and neck morphology in an aneurysm model in rabbits. Neurosci Lett 326: 46–50
20. Graves VB, Strother CM, Partington CR, Rappe A (1992) Flow dynamics of lateral carotid artery aneurysms and their effects on coils and balloons: an experimental study in dogs. AJNR Am J Neuroradiol 13: 189–196
21. Forrest MD, O'Reilly GV (1989) Production of experimental aneurysms at a surgically created arterial bifurcation. AJNR Am J Neuroradiol 10: 400–402
22. Reul J, Weis J, Spetzger U, Konert T, Fricke C, Thron A (1997) Long-term angiographic and histopathologic findings in experimental aneurysms of the carotid bifurcation embolized with platinum and tungsten coils. AJNR Am J Neuroradiol 18: 35–42
23. Fujiwara NH, Cloft HJ, Marx WF, Short JG, Jensen ME, Kallmes DF (2001) Serial angiography in an elastase-induced aneurysm model in rabbits: evidence for progressive aneurysm enlargement after creation. AJNR Am J Neuroradiol 22: 698–703